Biochimica et Biophysica Acta 1847 (2015) 576–586

Contents lists available at ScienceDirect

Biochimica et Biophysica Acta

journal homepage: www.elsevier.com/locate/bbabio

Electron transfer pathways from the S_2-states to the S_3-states either after a Ca^{2+}/Sr^{2+} or a Cl^-/I^- exchange in Photosystem II from *Thermosynechococcus elongatus*

Alain Boussac [a,*], A. William Rutherford [b], Miwa Sugiura [c,d,e]

[a] *I²BC, CNRS UMR 9198, CEA Saclay, 91191 Gif-sur-Yvette, France*
[b] *Department of Life Sciences, Imperial College, London SW7 2AZ, UK*
[c] *Proteo-Science Research Center, Ehime University, Bunkyo-cho, Matsuyama, Ehime 790-8577, Japan*
[d] *Department of Chemistry, Graduate School of Science and Technology, Ehime University, Bunkyo-cho, Matsuyama, Ehime 790-8577, Japan*
[e] *PRESTO, Japan Science and Technology Agency (JST), 4-1-8, Honcho, Kawaguchi, Saitama 332-0012, Japan*

ARTICLE INFO

Article history:
Received 27 November 2014
Received in revised form 25 March 2015
Accepted 29 March 2015
Available online 2 April 2015

Keywords:
Photosystem II
Oxygen evolution
Mn_4CaO_5 cluster
Spin state
EPR

ABSTRACT

The site for water oxidation in Photosystem II (PSII) goes through five sequential oxidation states (S_0 to S_4) before O_2 is evolved. It consists of a Mn_4CaO_5-cluster close to a redox-active tyrosine residue (Y_Z). Cl^- is also required for enzyme activity. By using EPR spectroscopy it has been shown that both Ca^{2+}/Sr^{2+} exchange and Cl^-/I^- exchange perturb the proportions of centers showing high ($S = 5/2$) and low spin ($S = 1/2$) forms of the S_2-state. The S_3-state was also found to be heterogeneous with: *i*) a $S = 3$ form that is detectable by EPR and not sensitive to near-infrared light; and *ii*) a form that is not EPR visible but in which Mn photochemistry occurs resulting in the formation of a $(S_2Y_Z^{\bullet})'$ split EPR signal upon near-infrared illumination. In Sr/Cl-PSII, the high spin ($S = 5/2$) form of S_2 shows a marked heterogeneity with a $g = 4.3$ form generated at low temperature that converts to a relaxed form at $g = 4.9$ at higher temperatures. The high spin $g = 4.9$ form can then progress to the EPR detectable form of S_3 at temperatures as low as 180 K whereas the low spin ($S = 1/2$) S_2-state can only advance to the S_3 state at temperatures ≥ 235 K. Both of the two S_2 configurations and the two S_3 configurations are each shown to be in equilibrium at ≥ 235 K but not at 198 K. Since both S_2 configurations are formed at 198 K, they likely arise from two specific populations of S_1. The existence of heterogeneous populations in S_1, S_2 and S_3 states may be related to the structural flexibility associated with the positioning of the oxygen O_5 within the cluster highlighted in computational approaches and which has been linked to substrate exchange. These data are discussed in the context of recent *in silico* studies of the electron transfer pathways between the S_2-state(s) and the S_3-state(s).

1. Introduction

The light-driven oxidation of water in Photosystem II (PSII) is a key step in photosynthesis, the process that is the main input of energy into biology and is thus responsible not only for the production of biomass including food, fiber and fuels (fossil and non-fossil) but also for putting O_2 into the atmosphere. PSII in cyanobacteria is made up of 17 membrane protein subunits and 3 extrinsic proteins. Although the PsbY subunit was not detected in [1] it was seen in [2] and [3]. Altogether these 20 subunits bear 35 chlorophylls, 2 pheophytins (Phe), 2 hemes, 1 non-heme iron, 2 plastoquinones (Q_A and Q_B), a Mn_4CaO_5 cluster, 2 Cl^-, 12 carotenoids and 25 lipids [1]. The excitation resulting from the absorption of a photon is transferred to the photochemical trap P_{680}, which is composed of four chlorophyll *a* molecules, P_{D1}/P_{D2} and Chl_{D1}/Chl_{D2}, and two pheophytin *a* molecules, Phe_{D1}/Phe_{D2}. Charge separation then occurs. After some picoseconds the positive charge is mainly stabilized on P_{D1} but this is often termed P_{680}^+. P_{680}^+ then oxidizes Y_Z, the Tyr161 of the D1 polypeptide, which in turn oxidizes the Mn_4CaO_5 cluster. On the electron acceptor side, the electron is transferred to the primary quinone electron acceptor, Q_A, and then to Q_B, a two-electron and two-proton acceptor, *e.g.* [4–6]. The Mn_4CaO_5 cluster accumulates oxidizing equivalents and acts as the catalytic site for water oxidation. The enzyme cycles sequentially through five redox states denoted S_n where *n* stands for the number of stored oxidizing equivalents. Upon formation of the S_4 state two molecules of water are rapidly oxidized, the S_0 state is regenerated and O_2 is released, *e.g.* [5–12].

The S_1-state is the dark-stable state and the S_2-state can be formed from the S_1-state either by illumination by one flash at room temperature or by continuous illumination between 140 K and 230 K where

Abbreviations: PSII, Photosystem II; Chl, chlorophyll; MES, 2-(N-morpholino) ethanesulfonic acid; P_{680}, primary electron donor; P_{D1} and P_{D2}, Chl monomer of P_{680} on the D1 or D2 side, respectively; Q_A, primary quinone acceptor; Q_B, secondary quinone acceptor; EPR, Electron Paramagnetic Resonance; ENDOR, Electron Nuclear Double Resonance

* Corresponding author.
E-mail address: alain.boussac@cea.fr (A. Boussac).

http://dx.doi.org/10.1016/j.bbabio.2015.03.006
0005-2728/

the S_1 to S_2 transition occurs whereas the electron transfer from Q_A^- to Q_B is blocked thus preventing a second turnover, [13,14] and references therein. It should be however mentioned that when centers are in the Q_B^- state prior to the illumination, the electron transfer from Q_A^- to Q_B^- can occur at temperatures as low as 180–190 K [14].

From EPR spectroscopy at helium temperatures, the S_2-state may appear heterogeneous, exhibiting two different ground state configurations depending on the conditions (reviewed in [15,16]). The first S_2-state configuration has a spin $S = 1/2$ and exhibits a multiline signal centered at $g \approx 2.0$, spread over roughly 1800 G and made up of at least 20 lines, each separated by approximately 80 G [17]. The S_2-state can also exhibit other broad EPR signals, either a derivative-like signal centered at $g \approx 4.1$ or more complex signals at lower magnetic fields (at higher g values) [18–20] also attributed to spin states $S = 5/2$ [21,22].

In the S_1-state, the refined structure of the crystallographic structure of the Mn_4O_5Ca [1] resembles a distorted chair including a μ-oxo-bridged cuboidal Mn_3O_4Ca unit with a fourth Mn attached to this core structure *via* two μ-oxo bridges involving O_4 and O_5 [1] (see also related computational studies [12,23–36]). ENDOR analysis and X-ray spectroscopy of the S_2 state in the $S = 1/2$ state have strongly suggested that the OEC contains one Mn^{III} ion and three Mn^{IV} ions [10,37–40]. Theoretical studies [29,32] gave a rationale for the interconversion between the low spin ($S = 1/2$) and high spin ($S = 5/2$) S_2-states: the two almost isoenergetic structures share the same coordination environment but the unique Mn^{III} ion is located on Mn1 in the low spin S_2-state whereas it is located on the non-core Mn4 in the high spin S_2-state. This switching of the +3 valence between the Mn4 and the Mn1 is suggested to occur together with a movement of O_5 that leaves its bridging position between Mn4 and Mn3 in the low spin S_2-state closing the cube by making a μ-oxo bridge between the Mn1 and the Mn3 in the high spin S_2-state [29,32].

The S_n-state cycle is strongly influenced both by the H-bonding network involving the first coordination sphere of the Mn_4CaO_5 cluster, in particular the D1-Asp61 residue (see below), and by the H-bonding network that extends well outside the first coordination sphere reviewed in [41–43]. Biochemical conditions that affect this H-bonding network also modify the S_2-state equilibrium between the low spin and high spin S_2-states of the Mn_4CaO_5 cluster. It has been suggested, *e.g.* [16], that the hydrogen bonding of W1 and W2, the terminal water molecules bound to Mn4, could play and important role in this equilibrium (see below).

The S_3-state is induced by 2 flashes at room temperature. The complete X-band EPR spectrum [44] was simulated assuming an $S = 3$ ground state [44,45]. A multi-frequency, multi-dimensional magnetic resonance spectroscopy study of this EPR detectable S_3-state showed that all four Mn ions were structurally and electronically similar, with a +4 formal oxidation state and in an octahedral local geometry [46]. The magnetism of the Mn_4CaO_5 complex was described in terms of pairwise exchange interactions between the four Mn ions. First, the coupling between the 3 Mn^{IV} ions in the cubane Mn_3CaO_4 part (including the Mn1, Mn2 and Mn3) were dominantly ferromagnetic, rendering this fragment high-spin ($S = 9/2$). Second, an antiferromagnetic coupling between the outer $Mn4^{IV}$ ($S = 3/2$) and the cubane subunit ($S = 9/2$) mediated by a more linear μ-oxo/μ-carboxylato bridging network, yields the experimentally observed ground spin state ($S = 3$) [46].

An oxo-oxyl mechanism for O–O formation was suggested based on computational chemistry before the high resolution structure of the site was known [23,24]. This model has then received support from subsequent spectroscopic and theoretical studies and has undergone some changes in the detail: the O–O bond is formed between a bridging oxygen radical, likely on O_5, and a bridging μ-oxo (the O originating from the terminal water ligand, W2, that was bound to Mn4 in the lower S_n-states) between Mn3 and Mn4 [9,23–27,29–31,46–48]. Despite a certain degree of consensus, several mechanistic features, details and questions remain to be verified, clarified and answered respectively. One specific problem is to understand the complexity of the reactions occurring on the S_2 to S_3 transition. It has been proposed that the formation of $Y_Z^{\bullet}$ in the low spin S_2-state leads to the reorientation of the dipole moment of the Mn_4CaO_5 cluster such that the locus of negative charge becomes directed toward W1, the other H_2O molecule that is bound to Mn4, and its hydrogen bonding partner, D1-Asp61, resulting into the deprotonation of W1 and the shift of the equilibrium low spin $S_2 \leftrightarrow$ high spin S_2 in favor the high spin configuration [49] (see also [26,27]). In these models only the high spin S_2-state was able to progress to the S_3-state and thus the low spin form of S_2 had to become high spin in order to advance [49,50]. These models slightly differ from those in which the structure of the S_2-state that advances to S_3 has a di-μ-oxo bridge between the Mn3 and Mn4 and an open cubane structure for the rest of the cluster and yet has the isolated Mn4 position with +4 valence [27], see also [39,40].

The low spin to high spin transition in the S_2-state can also be induced by near-infrared illumination at temperatures ≤ 150 K [22,51–54]. The S_3-state is also near-infrared sensitive [55–57]. Near-infrared illumination of the S_3-state at ≈4 K results in the formation of a split EPR signal attributed to a $(S_2Y_Z^{\bullet})'$ state formed by near-infrared-induced conversion of the Mn_4CaO_5 cluster into an "activated" state able to oxidize Y_Z and thus leading to the formation of a $(S_2Y_Z^{\bullet})'$-state at the expense of the S_3Y_Z-state [55]. However, the formation of the $(S_2Y_Z^{\bullet})'$ split signal is not accompanied by a decrease of the $S = 3$ S_3 signal amplitude (Boussac, unpublished, see also [46]), suggesting that the near-infrared photochemistry and the formation of the $S = 3$ signal does not occur in the same centers. The question arises whether this heterogeneity in the S_3-state is related to that known in the S_2-state.

Most of the electron pathways and mechanisms summarized above that result from *in silico* studies should be tested by *in vitro* experiments. Here, we have focused on the S_2 to S_3 transition using Photosystem II preparations that exhibit both the low spin and high spin states in S_2. The standard preparations of PSII purified from *Thermosynechococcus elongatus* (a thermophilic cyanobacterium with PSII almost identical to that of *Thermosynechococcus vulcanus* which provided the best resolved PSII crystal structure), does not exhibit a high spin S_2-state (see [52,58] for conditions where high spin S_2-states can be formed). Instead, we have used either PSII in which Sr^{2+} has been substituted for Ca^{2+} or I^- has been substituted for Cl^-. In both cases, a high proportion of high spin S_2-state is formed [58,59] possibly as a consequence of a modification of the H-bond network extending from the Ca site to the halide site close to the D1-Asp61 site, *e.g.* [16,59,60]. The results obtained mainly support or are consistent with predictions from the computational studies but several new phenomena are reported which need to be integrated into current models to add more chemical details to the events occurring during these transitions in the enzyme cycle.

2. Materials and methods

The *T. elongatus* strain used was the *ΔpsbA1ΔpsbA2* deletion mutant [61] constructed from the *T. elongatus* 43-H strain that had a His_6-tag on the carboxy terminus of CP43 [62]. The biosynthetic Ca/Sr exchange, PSII purification and the biochemical Cl/I exchange were achieved as previously described [48,63,64].

X-band cw-EPR spectra were recorded with a Bruker Elexsys 500 X-band spectrometer equipped with a standard ER 4102 (Bruker) X-band resonator, a Bruker teslameter, an Oxford Instruments cryostat (ESR 900) and an Oxford ITC504 temperature controller. Flash illumination at room temperature was provided by a Nd:YAG laser (532 nm, 550 mJ, 8 ns Spectra Physics GCR-230-10). PSII samples at 1.1 mg of Chl mL^{-1} were loaded in the dark into quartz EPR tubes and dark-adapted for 1 h at room temperature. Then the samples were synchronized in the S_1-state with one pre-flash. After a further 1 h dark-adaptation at room temperature the samples were frozen in the dark to 198 K and then transferred to 77 K. The samples were degassed at

198 K prior to the recording of the spectra. Near-infrared illumination of the samples was done directly in the EPR cavity at 4.2 K and was provided by a laser diode emitting at 820 nm (Coherent, diode S-81-1000C) with a power of 600–700 mW at the level of the sample (for approximately 1 min). Illuminations with visible light for approximately 5–10 s with a 800 W tungsten lamp filtered by water and infrared cut-off filters at temperatures close to 200 K were done in a non-silvered dewar in ethanol cooled down either with liquid nitrogen or with dry ice for illumination at 198 K. No artificial electron acceptors were added to avoid the oxidation of the non-heme iron which gives an EPR signal that overlaps with parts of the high spin EPR signals in S_2 and with the $S = 3$ S_3 signal. In separate experiments it was verified that essentially similar results were obtained in the absence and the presence of the electron acceptor phenyl-*para*-benzoquinone (not shown).

To study the S_1 to S_2 transition, after synchronization in the S_1-state as indicated above, the PSII samples were illuminated either at room temperature by one saturating laser flash or by a continuous illumination for a few seconds at low temperature. Then, the EPR spectra were recorded. The S_3-state was induced either directly in samples in the S_1-state by two saturating laser flashes given at room temperature or by a continuous illumination for a few seconds at low temperature of a sample already in the S_2-state. Then, the EPR spectra were recorded. The equilibria between the two S_2-states and the two S_3-states were studied by a further incubation of the S_2-samples and S_3-samples at the indicated temperatures for the indicated duration.

3 . Results

Formation of the S_2-state was monitored in Sr/Cl-PSII either after 1 flash given at room temperature (Fig. 1A) or after continuous illumination for 5 s at 198 K (Fig. 1B). The black spectra were recorded in the dark-adapted state, *i.e.* in the S_1-state, and the red spectra were recorded after illumination. The blue spectra are the "light"-*minus*-"dark" difference spectra. Two observations can be made from these spectra. Firstly, the illumination by 1 flash at room temperature induced the formation of the $S = 1/2$, Sr-type [65,66] multiline signal in a proportion of PSII centers and an $S = 5/2$ signal at $g \approx 4.9$ (turning point at $\approx$1385 G) in the other PSII centers (Fig. 1A). Secondly, the illumination at 198 K (Fig. 1B) also induced the formation of the Sr-type $S = 1/2$ multiline signal in a proportion of PSII centers but, here, an $S = 5/2$ signal at $g \approx 4.3$ ($\approx$1560 G) was formed in the other PSII centers instead of the $g \approx 4.9$ signal seen in Fig. 1A. It should be noted here that the $g \approx 4.9$ signal was reported earlier but misattributed to a component of the non-heme iron signal [57]. Upon the illumination at 198 K, a large Q_A^- $Fe^{2+}Q_B^-$ signal at $g \approx 1.6$ [13,14,67] was detected. This indicates that in the absence of an added artificial acceptor, Q_B^- was present in a large proportion of centers ($\approx$40%) in the dark-adapted *T. elongatus* PSII sample, as previously reported under comparable conditions [14, 68].

Fig. 1C shows the effect of annealing of the sample previously illuminated at 198 K. The black spectrum was recorded in the dark-adapted sample and the red spectrum was recorded after an illumination at 198 K followed by a brief annealing (1–2 s) at room temperature. The blue spectrum is the "hν 198 K + annealing"-*minus*-"dark" difference spectrum. This annealing resulted in the complete conversion of the $g \approx 4.3$ signal into the $g \approx 4.9$ signal with an amplitude for the $g \approx 4.9$ signal similar, or slightly larger than that in the 1 flash sample. After annealing, the amplitude of the S_2 multiline signal became also similar to that after the 1 flash at room temperature. The slightly larger S_2 multiline signal upon 198 K illumination than after flash illumination at room temperature was likely due to the expected smaller "miss parameter" under continuous illumination at 198 K when compared to that under flash illumination and possibly to imperfect synchronization leaving some centers in the S_1-state but with a reduced Tyr_D [69]. Consequently, the $g \approx 4.9$ signal was slightly larger after annealing than after the flash illumination. Nevertheless, since the S_2 multiline signal was slightly smaller upon annealing we cannot discard the possibility that in a very small fraction of centers a fast charge recombination between the high spin and low spin S_2 states and Q_A^- also occurred during the warming of the Sr/Cl-PSII. However, taken together and assuming that all centers are detected by EPR, these data show that both the $g \approx 4.3$ signal and the $g \approx 4.9$ signal correspond to a comparable proportion of PSII centers in the high spin S_2 configuration.

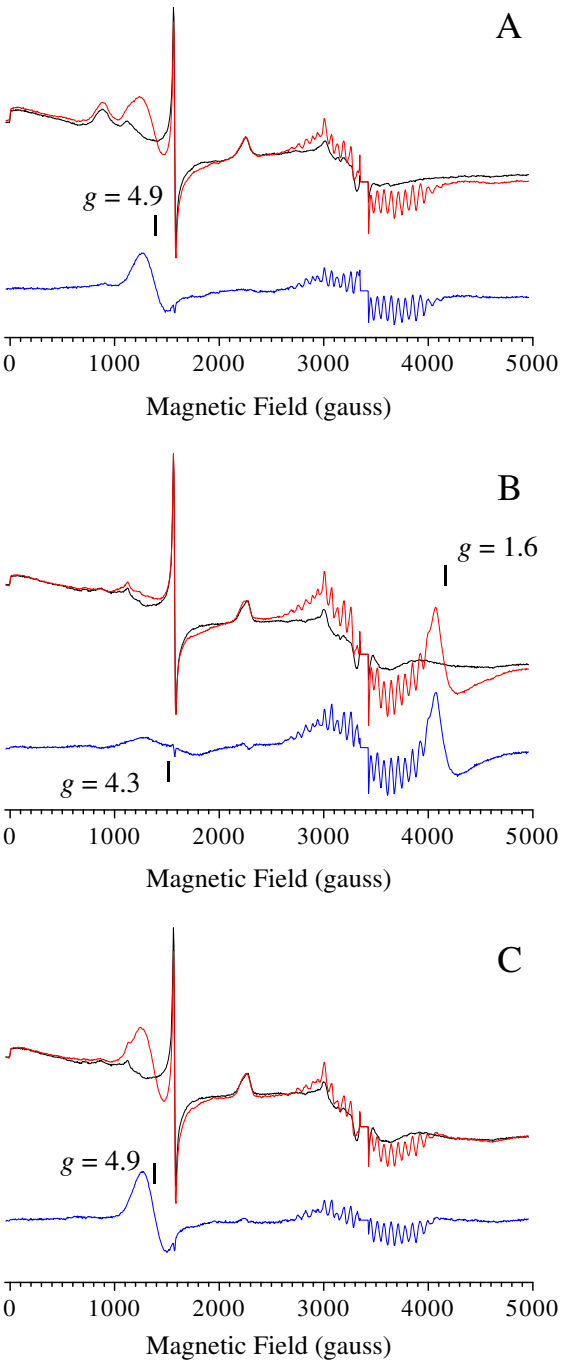

Fig. 1. EPR spectra recorded in Sr/Cl-PSII. In Panels A, B and C the black spectra were recorded in the S_1-state. Panel A: the red spectrum was recorded after 1 flash at room temperature. Panel B: the red spectrum was recorded after an illumination at 198 K. Panel C: the red spectrum was recorded after an annealing at room temperature of the sample previously illuminated at 198 K in Panel B. In the 3 panels, the blue spectra are the "light"-*minus*-"dark" difference spectra. The vertical scale is the same in the 3 Panels. Other instrument settings: [Chl] = 1.1 mg·ml^{-1}; Temperature, 9.6 K; modulation amplitude, 25 G; microwave power, 20 mW; microwave frequency, 9.4 GHz; modulation frequency, 100 kHz. The $Y_D^{\bullet}$ spectral region at $g \approx 2$ was deleted.

Fig. 2 shows a Sr/Cl-PSII sample which was first illuminated by 1 flash at room temperature and then further illuminated either by a second flash given at room temperature 1 s after the first flash (Fig. 2A) or by continuous illumination at 198 K (Fig. 2B). In Fig. 2A the black spectrum was recorded in the dark-adapted state, *i.e.* in the S_1-state, and the red spectrum was recorded after 2 flashes given at room temperature. The "2 flashes"-*minus*-"dark" difference spectrum in blue exhibits the most characteristic features of the $S = 3$ S_3 signal [44,46]. The main spectral signature of this signal is at ≈720 G ($g \approx 9.5$). The "2 flashes"-*minus*-"dark" spectrum also exhibit the $g \approx 4.9$ and multiline S_2 signals. The amplitude of the S_2 multiline signal is approximately 20% of that in Fig. 1B. This value is in agreement with the "miss parameter" ($\alpha \approx 10\%$, [63]) in the S_1 to S_2 and S_2 to S_3 transitions in Sr/Cl-PSII. In Fig. 2B the black spectrum was recorded after 1 flash at room temperature, *i.e.* in the S_2-state, and the red spectrum was recorded after a further continuous illumination at 198 K following the one flash illumination at room temperature. The blue spectrum is the "1 flash + hν 198 K"-*minus*-"1 flash" difference spectrum. Apart from the appearance of a large $Q_A^- Fe^{2+} Q_B^-$ signal at $g \approx 1.6$, again indicating the presence of Q_B^- prior to the illumination at low temperature [13,14,68], three important observations can be made in the difference spectra: *i*) the S_2 multiline signal formed by the 1-flash illumination was not affected by the further 198 K illumination; *ii*) the S_2 $g \approx 4.9$ signal fully disappeared upon the 198 K illumination; *iii*) the $S = 3$ S_3 signal was formed to the almost same extent as in the 2-flash sample. This is better illustrated in Panel D, which shows the magnetic field region where the main feature at $g = 9.5$ of the $S = 3$ S_3 signal contributes. The "1 flash + hν 198 K"-*minus*-"1 flash" difference spectrum in red has the same amplitude as the "2 flashes"-*minus*-"dark" difference spectrum in black. The differences on the right side of the $g = 9.5$ signal are due to different contributions from other signals in the base line like the S_2 $g = 4.9$ signal (see the full spectra in Panels A and B).

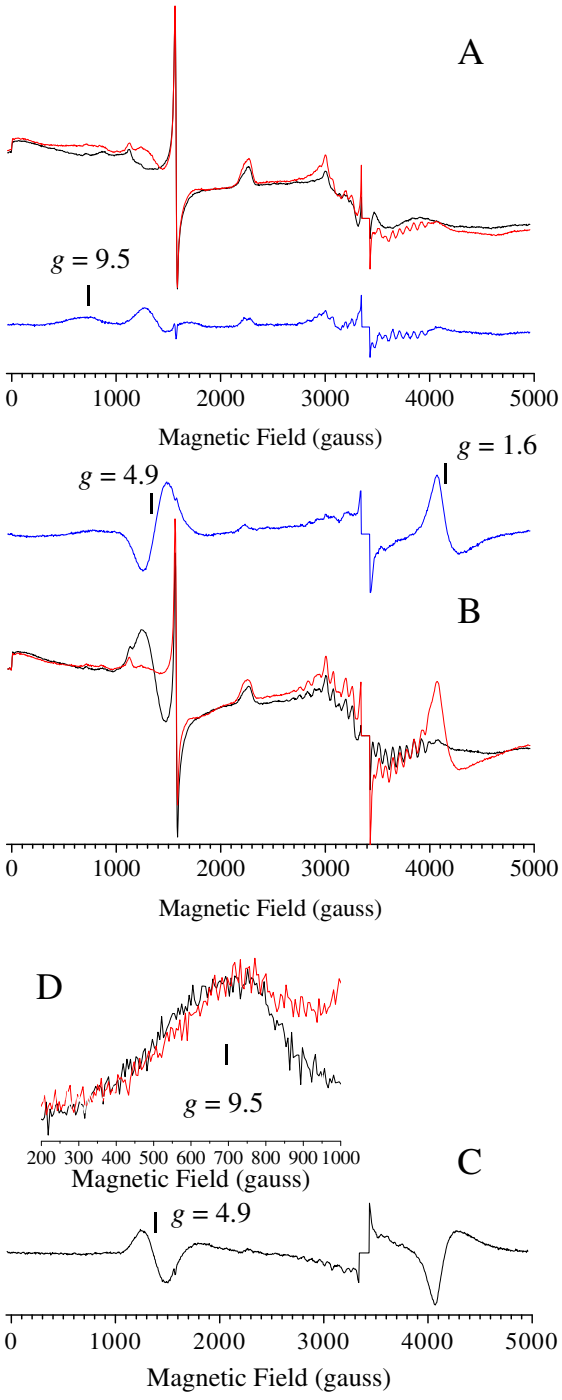

Fig. 2. EPR spectra recorded in Sr/Cl-PSII. In Panel A, the black spectrum was recorded in the S_1-state and the red spectrum after two flashes given at room temperature. In Panel B, the black spectrum was recorded after 1 flash at room temperature and the red spectrum after a further illumination at 198 K. The blue spectra in Panels A and B are the "red"-*minus*-"black" difference spectra. Panel C shows the difference spectrum "1 flash + hν 198 K + warming at 235 K"-*minus*-"1 flash room temp. + hν 198 K". Panels A, B and C have the same vertical scale and instrument settings as in Fig. 1. The $Y_D^{\cdot}$ spectral region at $g \approx 2$ was deleted. Panel D: zoom on the "1 flash + hν 198 K"-*minus*-"1 flash" difference spectrum in red and the "2 flashes"-*minus*-"dark" difference spectrum in black.

The full conversion of the high spin S_2-state into the EPR-detectable S_3-state at 198 K shows that the oxidation of Y_Z efficiently occurs in these centers at this temperature. Therefore, since the illumination of Sr/Cl-PSII at 198 K also induces the formation of a $S_2 Tyr_Z^{\cdot}$ state in centers in which the low spin S_2-state can be detected as a split signal after a further illumination at helium temperature following the 198 K illumination [57], the oxidation of Y_Z occurs efficiently in both the high spin S_2 and low spin S_2 configurations at 198 K.

In the S_2-state, the equilibrium at room temperature between the high spin configuration and the low spin configuration previously predicted in unmodified PSII [29,32] can be probed here in the Sr/Cl-PSII sample. Indeed, after 1 flash at room temperature and a further low temperature illumination the data above indicate that all the centers in the high spin configuration were converted into centers exhibiting the $S = 3$ S_3 signal, whereas the low spin S_2 configuration remained unaffected. After these two illuminations, warming of the sample to temperatures where the low spin ↔ high spin equilibrium [32] can occur should result in the formation of a $g \approx 4.9$ S_2 signal at the expense of the low spin S_2 population. The spectrum in Panel C of Fig. 2, which corresponds to the difference spectrum "1 flash + hν 198 K + warmed to 235 K"-*minus*-"1 flash room temp. + hν 198 K", shows that this indeed occurred. Despite the large change in the $Q_A^- Fe^{2+} Q_B^-$ signal at $g \approx 1.6$ that makes the detection of the S_2 multiline signal difficult in the magnetic field range above 3500 G, the spectrum in Panel C shows that the S_2 multiline signal disappeared in a proportion of the centers. From the amplitude of the negative multiline signal detected in the difference spectrum in Fig. 1C, approximately 25–30% of the multiline signal present prior to the warming procedure disappeared. It seems unlikely that the formation of the $g \approx 4.9$ S_2 signal, which occurs at the same time as a loss in the multiline signal, could be due to a back-reaction between the $S = 3$ S_3 state (the only S_3-state configuration formed here) and an electron from the reduced acceptor side. Indeed, as shown below, the lifetime of the S_3-state is too long ($t_{1/2} \gg 120$ s at room temperature, see below) to observe a decay during the ≈5 s warming process at 235 K used here.

The simplest explanation of the results in Fig. 2B is that the Sr/Cl-PSII centers in the $S = 5/2$ S_2 configuration are able to progress to S_3 at 198 K (this transition fully occurred down to at least 180 K, not shown), whereas those in the $S = 1/2$ S_2 configuration cannot advance to S_3 at 198 K.

In Fig. 3A, some consequences of the simple scheme proposed above were tested. Spectrum a in Fig. 3A is the difference spectrum "after"-*minus*-"before" near-infrared illumination at 4 K in the 2-flash sample; this corresponds to the maximum amount of the $(S_2Y_Z^{\bullet})'$ split signal that can be generated in the Sr/Cl-PSII. As described in the introduction section (Boussac, unpublished and [46]), this formation was not accompanied by a disappearance of the $S = 3$ S_3 signal, thus showing that the near-infrared induced conversion occurs in centers different from those exhibiting the $S = 3$ signal. Spectrum b in Fig. 3A shows the effect of near-infrared illumination at 4 K in a sample firstly illuminated by 1 flash at room temperature and then at 198 K by continuous light, *i.e.* conditions in which the $S = 3$ S_3 signal is fully generated from the high spin S_2-state, whereas the low spin S_2-state is not affected (see Fig. 1). In this case, a small split signal, different from that in spectrum a of Fig. 3A, was induced. This split signal likely corresponds to a $(S_1Y_Z^{\bullet})'$ split signal formed from the low spin S_2-state [70]. Indeed, a similar split signal could be induced upon near-infrared illumination at 4 K in a 1 flash sample (not shown but see the supplementary material). A careful examination of spectrum b in Fig. 3A also shows that in a small proportion of centers the low spin S_2-state (a decrease in the S_2 multiline signal) was converted into the high spin S_2-state by near-infrared illumination at this low temperature, *i.e.* at a lower temperature than in previous studies [71].

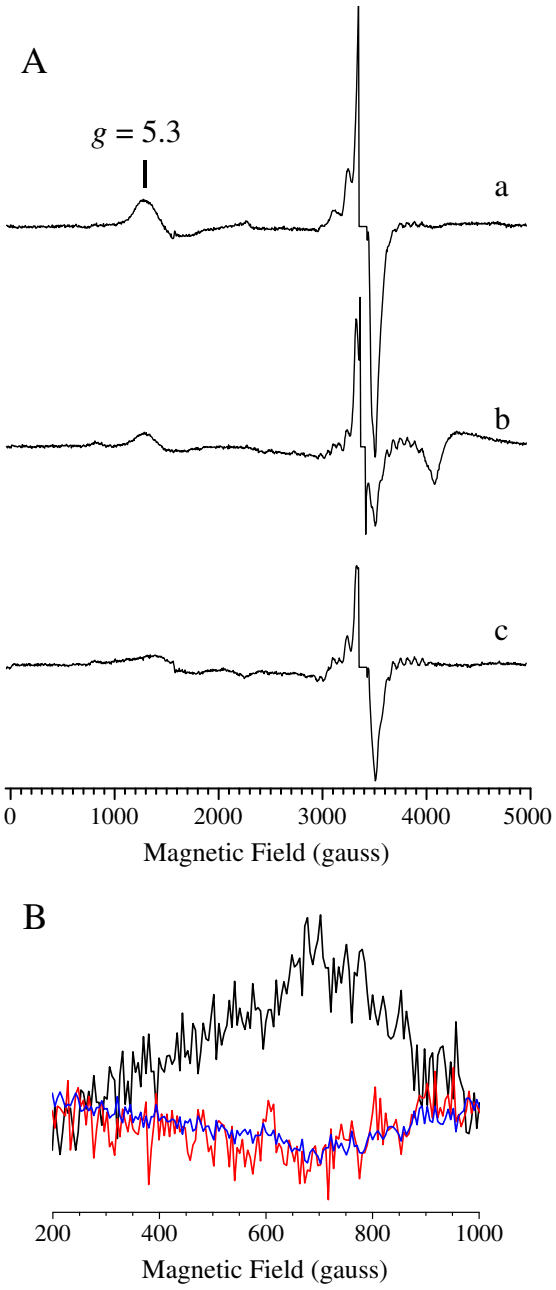

Fig. 3. EPR spectra recorded in Sr/Cl-PSII. Panel A, spectrum a is the difference spectrum "after"-*minus*-"before" near-infrared illumination at 4 K in the 2-flash sample. Panel A, spectrum b is the difference spectrum "after near-infrared illumination at 4 K"-*minus*-"before near-infrared illumination" in a sample first illuminated by one flash at room temperature and then by 198 K illumination. Panel A, spectrum c is the difference spectrum "after near-infrared illumination at 4 K"-*minus*-"before near-infrared illumination" in a sample previously illuminated by one flash at room temperature then by an illumination at 198 K followed by an annealing at 235 K. Same instrument settings as in Fig. 1. The $Y_D^{\bullet}$ spectral region at $g \approx 2$ was deleted. Panel B, the black spectrum is the difference spectrum "1 flash at room temperature + hν 198 K"-*minus*-"1 flash at room temperature". Panel B, the red spectrum is the difference spectrum "1 flash at room temperature + hν 198 K + annealing"-*minus*-"1 flash at room temperature + hν 198 K". Panel B, the blue spectrum is the black spectrum times −0.3. Same instrument settings as in Fig. 1.

Spectrum c in Fig. 3A shows the effect of near-infrared illumination at 4 K on a sample illuminated by 1 flash at room temperature followed by an illumination at 198 K and then a brief warming (≈5 s) at 235 K. The temperature of 235 K was chosen because this is a temperature at which the Mn_4 cluster and its protein and H-bond environment is not fully frozen and thus equilibria involving structural changes and proton movements can still occur, *e.g.* [72]. In this sample, the $(S_2Y_Z^{\bullet})'$ split signal was again detected. The most obvious explanation for the formation of the near-infrared sensitive S_3-state upon annealing to 235 K is that the two S_3 configurations equilibrate at this temperature. Spectrum c also shows that, as with spectrum b, both the $(S_1Y_Z^{\bullet})'$ split signal and the high spin configuration of the S_2-state were formed from the low spin multiline S_2-state by the near-infrared illumination.

After taking into account the contribution of the $(S_1Y_Z^{\bullet})'$ split signal formed in centers in the low spin S_2-state (spectrum b in Fig. 3A) in spectrum a and spectrum c, the proportion of centers in the near-infrared sensitive S_3 configuration state can be estimated to be about 40 ± 10% of that after 2 flashes at room temperature. Altogether, the data in spectra a, b and c show the existence of an equilibrium at temperatures as low as 235 K between the centers exhibiting the $S = 3$ S_3 signal and those which are not EPR detectable but in which the $(S_2Y_Z^{\bullet})'$ split signal can be induced by near-infrared illumination. Importantly, since the near-infrared sensitive S_3-state was formed at 235 K from the centers exhibiting the $S = 3$ S_3 signal formed at 198 K, it seems unlikely that this is an intermediate state between the high spin S_2-state and the EPR detectable S_3-state.

Spectrum b in Fig. 3A also shows that the $Q_A^{-}Fe^{2+}Q_B^{-}$ signal decreased upon near-infrared illumination. This is often observed upon near-infrared illumination and we have not yet an explanation for this phenomenon. A change in the electronic configuration of the non-heme iron resulting in a decoupling of the magnetic interaction between the quinone radicals and the metal could be involved. However, no EPR signals originating from uncoupled radicals were detected. This effect will be addressed in future work.

The black spectrum in Fig. 3B that is the difference spectrum "1 flash at room temperature + hν 198 K"-*minus*-"1 flash at room temperature" shows the main feature of the $S = 3$ EPR signal, on an expanded scale, that can be induced with this protocol. From the results above, the warming at 235 K of this sample is expected to result in a decrease of this signal due the equilibrium between the two S_3 forms. Indeed, the red spectrum in Fig. 3B that is the difference spectrum "1 flash at room temperature + hν 198 K + warming at 235 K"-*minus*-"1 flash at room temperature + hν 198 K" shows a negative $S = 3$ EPR signal. The blue spectrum that is the black spectrum times −0.3 shows that approximately 30% of the S_3 signal disappeared upon the warming at 235 K, a value close to that estimated from the appearance of the $(S_2Y_Z^{\bullet})'$ split signal induced by near-infrared illumination upon the warming at 235 K.

The equilibrium between the two S_3-states, *i.e.* one that is not near-infrared sensitive but is detectable by EPR and the other that is

near-infrared sensitive but not detectable by EPR, was further monitored in the experiment reported in Fig. 4. In this experiment the Ca/Cl-PSII sample (black symbols), the Sr/Cl-PSII sample (red symbols) and the Ca/I-PSII sample (blue symbols) were illuminated by two flashes at room temperature. Then, the 2-flash samples were frozen after variable dark periods at room temperature following the two flashes and the EPR spectra were recorded before and after a further near-infrared illumination. No artificial electron acceptor was added to allow the S_3-state to decay by charge recombination with an electron stored on the acceptor side. The amplitude of the $S = 3$ S_3 signal was monitored by measuring the amplitude of the main feature at low field (around 800 G). The amount of centers not EPR-detectable but near-infrared sensitive was monitored by measuring the amplitude of the $(S_2Y_Z^{\bullet})'$ split signal and that of the $g \approx 5.3$ signal, both of which are generated by near-infrared illumination [58,73]. Within the accuracy limit of the experiment, Fig. 4 shows that all species, in a given sample, decayed with the same rate thus reinforcing the idea that the two S_3-states are in equilibrium at room temperature. As previously observed, the decay of S_3 was much slower in Sr/Cl-PSII than in Ca/Cl-PSII [74] whereas in Ca/I-PSII it is shown here to be similar to that in the native Ca/Cl-PSII.

The formation of a high spin S_2-state in PSII from *T. elongatus* is also favored by a Cl/I exchange (Ca/I-PSII) [59]. Fig. 5 shows the effect of 1 flash given at room temperature (Fig. 5A) or the effect of a 198 K illumination (Fig. 5B) using Ca/I-PSII (the amplitudes of the spectra in Panel B was divided by two when compared to those in Panel A to allow the display of the split signal in Panel B). The black spectra were recorded in the dark-adapted state, *i.e.* in the S_1-state, and the red spectra after illumination. The blue spectra are the "light"-*minus*-"dark" difference spectra. As in Sr/Cl-PSII, the amplitudes of the low spin S_2 multiline signal were similar in both conditions but, in contrast to Sr/Cl-PSII, in Ca/I-PSII the same high spin S_2 signals at $g \approx 4.09$ and $g \approx 9.5$ (725 G) were observed whatever the temperature at which the S_2-state was formed (note that the signal at $g \approx 9.5$ was not detected in [59] due to the superimposition of the non-heme iron signal in this previous work).

Panel A in Fig. 6 shows the effect of 2 flashes given at room temperatures and the effect of a further near-infrared illumination using Ca/I-PSII. The black spectrum was recorded in the dark-adapted state, the red spectrum after 2 flashes given at room temperature and the blue spectrum is the spectrum recorded after a further near-infrared illumination at 4 K of the 2-flash sample. An S_3 signal with the main feature at $g \approx 12.5$ ($\approx$540 G) was detected in the 2-flash sample and, as in the other types of PSII studied here, the near-infrared illumination resulted in a $(S_2Y_Z^{\bullet})'$ split signal without affecting the main features of the S_3 signal.

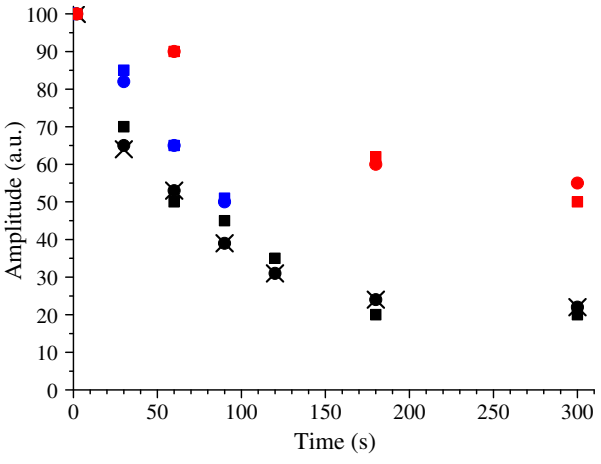

Fig. 4. Kinetics of the decay in the dark and at room temperature measured after two flashes in Ca/Cl-PSII (black symbols), Sr/Cl-PSII (red symbols) and Ca/I-PSII (blue symbols) of the $g = 5.3$ signal (crosses), of the split signal (full circles) and of the $S = 3$ S_3 signal (full squares). Same instrument settings as in Fig. 1 except for the temperature which was 4.2 K.

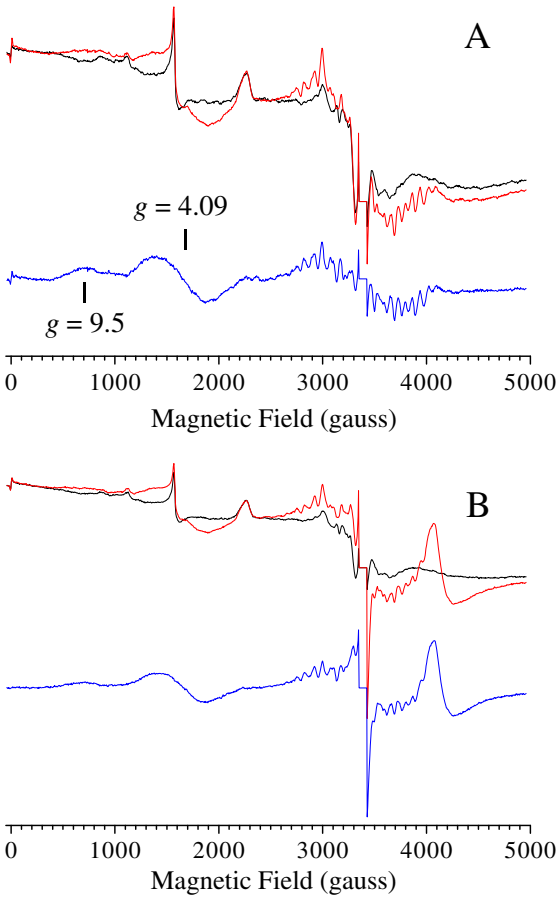

Fig. 5. EPR spectra recorded in Ca/I-PSII. In Panels A and B the black spectra were recorded in the S_1-state. Panel A: the red spectrum was recorded after 1 flash at room temperature. Panel B: the red spectrum was recorded after an illumination at 198 K. The blue spectra are the "light"-*minus*-"dark" difference spectra. The vertical scale in Panel B is twice that in Panel A. Other instrument settings as in Fig. 1.

Fig. 6B shows the effect of a further 198 K illumination (for $\approx$5 s) given to the 1-flash Ca/I-PSII. The black spectrum is a re-plot of the spectrum recorded in the 1-flash sample and the red spectrum was recorded after a further 198 K continuous illumination. A large $S_2Tyr_Z^{\bullet}$ split signal, much narrower than in Ca/Cl-PSII and Sr/Cl-PSII [57], was induced. At the same time, the multiline signal amplitude decreased whereas the $g \approx 4.09$ S_2-signal did not decrease showing, that in Ca/I-PSII, the $S_2Tyr_Z^{\bullet}$ is formed only in centers in the low spin S_2 configuration, as seen in the Sr/Cl-PSII. In contrast to Ca/Cl-PSII and Sr/Cl-PSII [45,54,75], the $S_2Tyr_Z^{\bullet}$ split signal induced in the S_2-state by visible light in Ca/I-PSII is stable at 198 K so that a further illumination with visible light at 4 K was not required for inducing this signal.

The second important difference with the Sr/Cl-PSII is that in Ca/I-PSII centers neither the high spin S_2 configuration nor the low spin S_2 configuration are able to progress to the S_3 state upon illumination at 198 K. The narrow split signal seen after 198 K illumination in Fig. 5B is similar to the split signal induced after the illumination at 198 K of the 1-flash sample (Fig. 6B) with an amplitude that is approximately half of that in the 1-flash sample that was further illuminated at 198 K. The formation of this split signal that required two charge separations at 198 K could be induced in centers with Q_B^- present prior to the illumination. The first illumination would produce the $Q_A^-Fe^{2+}Q_B^-$ state. Then, after the electron transfer from Q_A^- to Q_B^- at 198 K in a proportion of centers [14], Q_A would be again available to accept an electron. The possibility that this split signal originates from a $S_nY_Z^{\bullet}$ state different

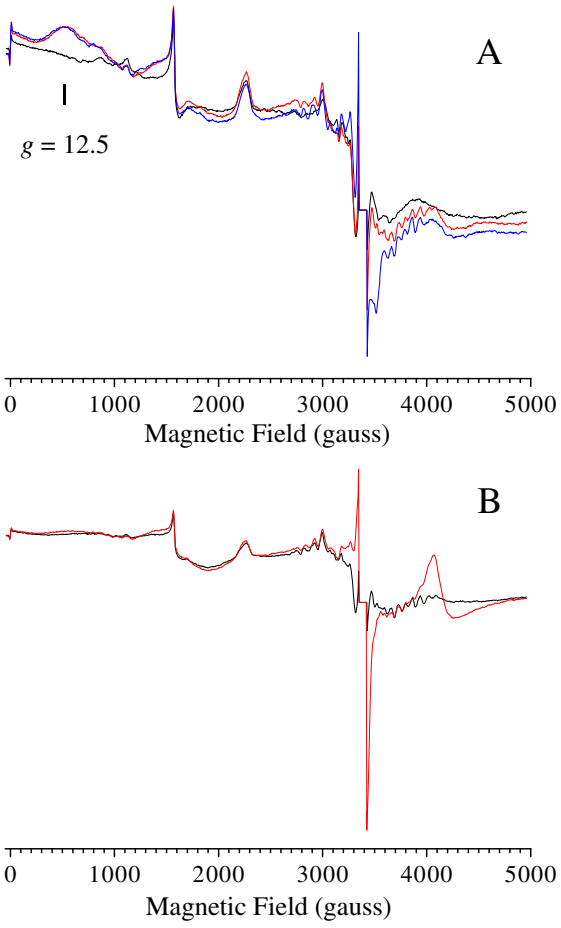

Fig. 6. EPR spectra recorded in Ca/I-PSII. Panel A: the black spectrum was recorded in the S_1-state, the red spectrum was recorded after 2 flashes given at room temperature and the blue spectrum was recorded after a further near-infrared illumination at 4 K. Panel B: the black spectrum was recorded after 1 flash given at room temperature and the red spectrum after a further illumination at 198 K. The vertical scales in Panels A and B are the same as in Panels A and B in Fig. 5, respectively. Other instrument settings as in Fig. 1.

from the $S_2Y_Z^{\bullet}$ state does not seems likely because it does not resemble the $S_0Y_Z^{\bullet}$, the $S_1Y_Z^{\bullet}$ generated by visible light illumination of Ca/I-PSII in the S_0-state and S_1-state, respectively, the $(S_1Y_Z^{\bullet})'$ state nor the $(S_2Y_Z^{\bullet})'$ state generated by near-infrared illumination of Ca/I-PSII in the S_2-state and S_3-state, respectively (see supplementary material).

4. Discussion

The electron pathways between the S_2-state and the S_3-state have been investigated in PSII from *T. elongatus* in which either the native Ca^{2+} in the active site was replaced by Sr^{2+} [2,63,74] or the native Cl^- was replaced by I^- [59,76]. These modifications allow the S_2-state to be generated in both high spin and low spin configurations. The Ca binding site and the Cl binding site are localized within the same H-bonding network [1,2,76] and this probably explains why modification of these ions produce some effects in common, including favoring the formation of a high spin S_2-state, *e.g.* [16]. Although a high proportion of high spin S_2-state is formed in both Sr/Cl-PSII and Ca/I-PSII, these two types of sample however, do differ significantly from each other. Similarities, differences and consequences on the electron pathways between the S_2-state and the S_3-state are summarized in Fig. 7 and are discussed below.

In this study, the transitions between some of the S-states were generated at high temperatures above 180 K while the S-states themselves were identified using their EPR characteristics at helium temperatures. A reviewer points out that the use of low temperatures may affect distributions of spin states *etc.* and this could skew the interpretation. This problem is intrinsic to all studies in which cryogenic temperatures are used (EPR, EXAFS, UV–vis, vibrational spectroscopy and X ray crystallography) and while the problem has remained potential rather than real in nearly all cases, it cannot be wholly eliminated. Most researchers using these methods are quite aware of the problem. In Photosystem II, an attempt was made to address this question using EXAFS [77] and only minor differences were recorded between 290 K and 18 K. No strong conclusions concerning temperature dependence were drawn. In the present work, the effect of low temperatures in some EPR is not ignored. It is discussed with regard to temperature dependence of redox transitions and deprotonation reactions and is dealt with explicitly in theoretical studies, *e.g.* [32].

In Sr/Cl-PSII, in addition to the modified $S = 1/2$ multiline signal [65,66], two different $S = 5/2$ EPR signals, corresponding to two high spin configurations, can be detected in the S_2-state: a $g \approx 4.9$ state induced by flash illumination at room temperature and a $g \approx 4.3$ signal induced by illumination at 198 K. The $g \approx 4.3$ state seems to be a precursor state of the $g \approx 4.9$ state since warming of the sample after the illumination at 198 K induces the conversion of the $g \approx 4.3$ to $g \approx 4.9$ form. Remarkably, the centers exhibiting the $g = 4.9$ form of S_2 are able to advance to S_3 down to temperatures as low as 180 K, while those showing the multiline signal behave "normally" in that they are unable to advance to S_3 at these low temperatures.

It is well established that the S_2 to S_3 transition involves a deprotonation, with the proton release thought to precede electron transfer from the cluster to $Y_Z^{\bullet}$, *e.g.* [78–82], see also *e.g.* [6,41–43] for more recent relevant reviews, and for theoretical treatments see [26,27,49]. Since the proton released corresponds (at least formally) to the positive charge already accumulated on the S_1 to S_2 transition, it seems unlikely that S_3 can be formed without a prior deprotonation event. This deprotonation step is considered to be responsible for the block in S_2 to S_3 transition at low temperature temperatures close to 200 K (*e.g.* [26,49,72]). The observation that the $g = 4.9$ form of S_2 is able to advance to S_3 suggests that this new form of S_2 may be deprotonated. This suggestion is apparently contradicted by the fact that the proton release pattern in Sr/Br-PSII [48] is essentially similar to that of the native Ca/Cl-PSII [78–82] (*nb.* the preparations used for the deprotonation experiments did show the same high spin to low spin ratios in S_2 as seen with the present preparations (not shown)). Nevertheless, the possibility remains that the $g = 4.9$ form of S_2 does represent a state in which a proton movement has occurred in the vicinity of the active site and yet the proton is not released to bulk. The relaxation of the low temperature form of the high spin state (showing the $g = 4.3$ signal) at high temperatures to form the $g = 4.9$ high spin configuration could represent this local deprotonation event.

An alternative possibility that is worth considering is the following: rather than a true proton movement, the proton to be released is primed on the $g = 4.1$ to $g = 4.9$ step by tuning of H-bonds lowering the energy barrier for deprotonation. This could allow deprotonation at lower temperatures. In recent models based on the crystal structure and computational chemistry, it was suggested that the water W1, which is liganded between Mn4 and Asp61 undergoes deprotonation on the S_2 to S_3 transition, being triggered by changes in the hydrogen bonding network that connects to Y_Z [25–27,30–32,49]. There is precedence for low temperature deprotonation reactions in PSII associated with tyrosine oxidation [53,83]. Unusually short, single-well H-bonds exist between the Tyr-OH and the histidine that act as its H-bonding partner [84,85]. For Y_Z, the tuning is achieved by additional H-bond donation to the phenolic by water molecules. Thus the $g = 4.1$ to the $g = 4.9$ transition could involve water movement, halide movement and/or small changes in the protein *etc.*, leading to a rearrangement of the H-bond network that results in a shortening of a specific H-bond or bonds, rather than a deprotonation reaction *per se*. In this case, the deprotonation itself would actually occur rapidly at low temperature during the S_2 to S_3 transition, prior to oxidation of the cluster.

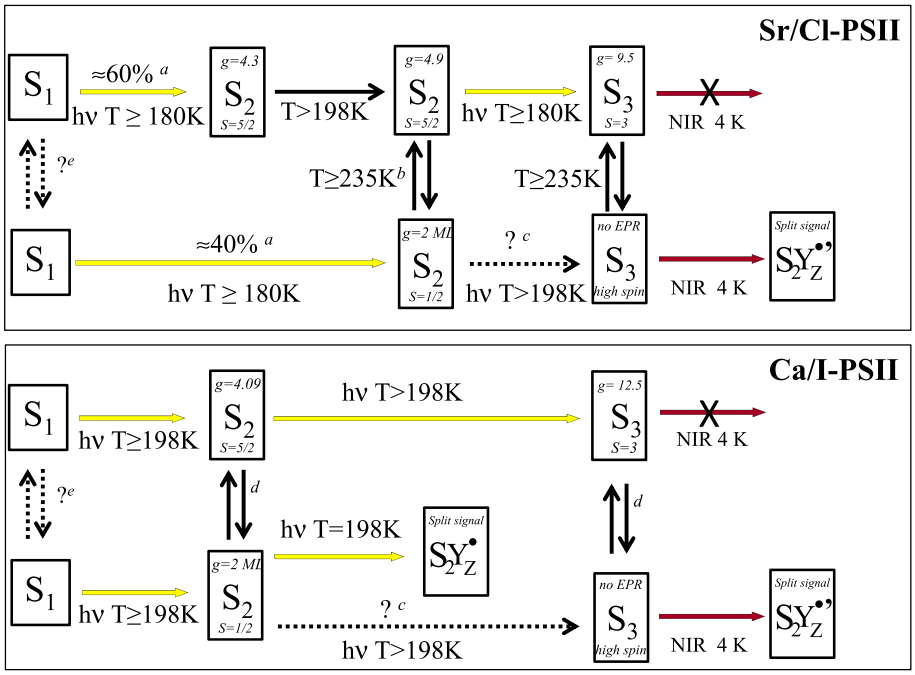

Fig. 7. Electron pathways from the S_1-state to the S_3-state in Sr/Cl-PSII and Ca/I-PSII based on the literature and on the present work. [a]This percentage is based on the proportion of centers in which the split $(S_2Y_Z^{\bullet})'$ signal induced by near-infrared illumination in the S_3-state is detected. [b]Equilibrium as proposed in [30,32]. [c]The question mark indicates that the direct route from the low spin S_2 configuration to the S_3 configuration not detectable by EPR cannot be discarded. [d]Equilibrium postulated from the literature in Ca/Cl-PSII and the present work in Sr/Cl-PSII. It cannot be probed here because the S_2 to S_3 transition occurs at the same temperature for the high spin S_2 and low spin S_2 configurations. [e]Possible heterogeneity in S_1. The equilibrium between low spin S_2 and $g = 4.9$ form of the high spin form may occur with the $g = 4.3$ form as an intermediate. The transition from the $g = 4.3$ form to the $g = 4.9$ most likely involves proton movement.

The high spin and low spin forms of S_2 equilibrate at temperatures of 235 K and above. This is seen as the appearance of the $g = 4.9$ form at the expense of the low spin form. It seem possible, even likely, that this equilibrium occurs *via* formation of the state that gives rise to the $g = 4.3$, the unrelaxed high spin form but the conditions of the experiment do not allow the intermediate state to be detected.

In the Sr/Cl-PSII, the centers exhibiting the low spin multiline signal do not advance to S_3 at 198 K. This is also a demonstration that the low spin to high spin transition in S_2 does not occur at a significant rate at this temperature. In the native Ca/Cl-PSII, although the $S = 1/2$ and $S = 5/2$ configurations are computed to be almost isoenergetic and in equilibrium at room temperature [30,32,35,36,49]. It was predicted that due to the slight endergonicity of the low spin S_2 to high spin S_2 transition (with $\Delta G \approx 1.1$ kcal mol^{-1}) and the relatively large activation barrier (with $\Delta G^{\#}$ of ≈ 10.6 kcal mol^{-1}), the half-time of the low spin to high spin conversion becomes very slow at low temperature [32]. The data shown here in Sr/Cl-PSII are fully consistent with these predictions. Indeed, nevertheless the presence of both high spin and low spin forms in S_2 in the Sr sample which indicates that they are likely to be similar in energy and nevertheless the formation of $Y_Z^{\bullet}$ in both the high spin and low spin forms in S_2, no S_2 multiline signal disappeared upon 198 K illumination. These observations strongly indicate that the low spin to high spin conversion does not occur at 198 K.

When the high spin S_2-state had been converted to the S_3-state by illumination at 198 K, the remaining S_2 state in its low spin form was stable at this temperature and the low spin configuration only equilibrated, forming the high spin configuration of S_2, at temperatures significantly higher than 198 K. These results, when taken with the observation that the high spin and the low spin S_2 configurations are both observed after an illumination at 198 K, indicates that two different configurations also exist in the S_1-state as specific precursors of the high spin S_2-state or the low spin S_2-state. Such a situation has been implicit in the EPR literature for decades and has recently been proposed based on computational analysis of the crystal structure, *e.g.* [12]. This is worthy of future study to see if the two S_1 states are distinguishable spectroscopically.

The results also show the existence of a heterogeneity in the S_3-state in the samples studied (Sr/Cl-PSII and Ca/I-PSII) as well as in native PSII [46]: *i*) the well-studied EPR detectable $S = 3$ form and *ii*) a form that is not seen by EPR but which is sensitive to near infrared light giving rise to a $(S_2Y_Z^{\bullet})'$ split signal. After 2 flashes at room temperature, the $S = 3$ S_3 EPR signal is observed in a proportion of centers comparable to that in which the high spin state was present in the S_2-state. The percentage of centers that were not EPR detectable in S_3 were estimated to be 30–40% by comparing the area of the field-swept echo spectrum of the near infrared-induced $(S_2Y_Z^{\bullet})'$ split signal to that of the $Y_D^{\bullet}$, (*e.g.* [86] for a similar procedure aimed at quantifying the split signal in Ca-depleted PSII). The two forms of S_3 states seem to be in equilibrium at 235 K. This conclusion was drawn from the observation that warming to 235 K of samples containing only the EPR-detectable $S = 3$ form of S_3 resulted in a decrease in this form and an increase in the other (EPR invisible) form, as monitored by the near infrared-induced $(S_2Y_Z^{\bullet})'$ split signal (Fig. 3A and B). The equilibrium proportions of each form were close to those seen for the two forms when generated by flashes at room temperature. The findings here thus indicate that the invisible S_3-state is not a precursor of the EPR detectable S_3-state in disagreement with a recent suggestion [46].

It is tempting to relate the apparently similar proportions of the two configurations detected in S_2 and S_3 and conclude that they have a common structural determinant: flexibility in the cluster as suggested for the S_2-state. This is probably too simplistic since the redox state of the Mn ion has important influences of the structure as well as reactivity. Computational chemistry has suggested that the high spin form of S_2 is an obligatory intermediate in the S_2 to S_3 transition [30,32]. Here we report that the S_3 state is formed at low temperature only from the high spin form and that the low spin form of S_2 only advances when it is possible to equilibrate, thus allowing formation of the high spin form. These results seem to be at least consistent with a high spin S_2

as an obligatory intermediate in S_3 formation. However, we also found a second form of the S_3 state that was formed from the EPR detectable $S = 3$ S_3-state when equilibration could occur (at 235 K). The second form of S_3, which is characterized as giving rise to a split $(S_2Y_Z^{\bullet})'$ signal as a result of photochemical excitation of the Mn cluster, also appears to be a high spin state based on the EPR spectrum of the S_2-state that appeared when the split $(S_2Y_Z^{\bullet})'$ signal was generated [73]. One possibility to explain the two S_3 configurations is that the protonation of a group would be responsible for this heterogeneity. However, the amplitude of the near-infrared-induced $(S_2Y_Z^{\bullet})'$ split signal remained unaffected between pH 5.5 and 8.2 making this possibility unlikely. Note that in spinach PSII the yield of the split signal decreased below pH ≈ 5 and above pH ≈ 7.5 [87].

While our data are consistent with the computational chemistry models, from the results above we cannot totally rule out other pathways such as the direct progress from the low spin S_2 toward the EPR silent S_3-state without populating the high spin S_2 configuration. However, this would be at odds with the theoretical studies mentioned above [30,32] and it seems unlikely that the presence of Sr, in the present work, rather than Ca in the native PSII can explain this discrepancy. Furthermore, the fact that in native Ca/Cl-PSII two populations of S_3 similar to those observed here are present and yet the S_2 state shows little high spin form argues against the simplistic argument based on proportionality that the high spin S_2 advances to the EPR detectable form of S_3, while the low spin S_2 advances directly to the EPR invisible S_3 state.

Another computational study put forward a slightly different model for the S_2 to S_3 transition: a S_2-state having an intermediate structure with an open cubane and a di-μ-oxo bridge between the Mn4 and the Mn3, as in the low spin S_2 configuration, but with the Mn^{III} on the pendant Mn4 [27], as in the high spin S_2 configuration for [30,32]. This model was less directly influenced by the EPR studies on high spin and low spin forms of S_2 so we do not consider it justified to use the ambiguity it provides to put forward the idea that the low spin S_2 transitions to S_3 without going through the high spin transition. However, the present work does not allow us to rule out that possibility.

The conclusion made here seems in contradiction with a previous study done in Ca/Cl-PSII from plant in which it was proposed that the multiline conformation was an intermediate state between the $g = 4.1$ S_2 conformation and the S_3-state [88]. However, the main experiment in [88] actually showed that, upon an illumination at 226 K of a sample in the S_2-state, the multiline signal remained unaffected whereas the $g = 4.1$ signal disappeared and the S_3 signal appeared. Upon illumination at higher temperatures, the multiline signal disappeared without a matching increase in the formation of the S_3 signal which continued to follow the loss of the $g = 4.1$ signal. All these observations are in agreement with the model proposed here and suggest that, very likely, the same events in the S_2 to S_3 transition occur in plant PSII and cyanobacterial PSII.

The data in Fig. 2 also allow us to give some rationale to a previously unexplained result concerning the $S_2Y_Z^{\bullet}$ split signal formed from the S_2-state. This $S_2Y_Z^{\bullet}$ split signal is generated in samples after one flash at room temperature to form the S_2-state, followed by an illumination at 198 K with visible light. Upon the 198 K illumination, the $S_2Y_Z^{\bullet}$ state is not stable and decays in part during the time required for the transfer of the EPR tube into the cryostat [53,54,57,75]. The $S_2Y_Z^{\bullet}$ split signal can then be fully regenerated by an illumination by visible light at helium temperatures in centers that had previously been in the $S_2Y_Z^{\bullet}$ state at 198 K. Given the prediction [49] that it is the formation of $Y_Z^{\bullet}$ that triggers the low spin S_2 to high spin S_2 transition, and given the demonstration here that only the S_2 high spin configuration is able to progress to S_3 at 198 K, this explains why the $S_2Y_Z^{\bullet}$ split signal induced by visible light illumination was only detected in centers in the low spin S_2 multiline configuration and not in those in the high spin S_2 configuration.

As mentioned earlier [24–27], the halide is thought to bind to the water molecule W1 that is bound to Mn4 and thought to become H_3O^+ on the S_2 to S_3 transition. It is therefore expected that, in addition to the effect on the high spin S_2 to low spin S_2 ratio seen here, the halide exchange modifies the S_2 to S_3 transition. It is shown here that this is indeed the case. In Ca/I-PSII, the same proportion of high spin S_2 signal was detected whatever the temperature of formation of the S_2-state. Although we cannot strictly compare the high spin signal formed in Ca/I-PSII with the high spin signals formed in Sr/Cl-PSII, the $g = 4.09$ is more similar to the $g = 4.1$ signal than to the $g = 4.9$ signal. An important difference with the Sr/Cl-PSII is that in the Ca/I-PSII sample the high spin form of S_2 is unable advance to S_3 at 198 K. It has been observed that the lag phase at 292 nm in the S_3 to S_0 transition, which is attributed to the first proton release occurring in this transition, was much slower in Ca/I-PSII [59]. It is possible that the two phenomena, the longer lag phase and the inhibition of the S_2 to S_3 transition at low temperatures, originate from the same modification of the water/proton channel, and both involve the halide. The finding here that the $S_2Y_Z^{\bullet}$ split signal that is induced by visible light in S_2 is stable at 198 K in Ca/I-PSII, as shown here (Fig. 6) may be a further consequence of iodide-induced modification of the hydrogen bonding environment.

The electron pathways found here are summarized in Fig. 7. These results provide several new insights into the electron pathways from the S_1-states to the S_3-states. Firstly, it provides the first experimental evidence for a S_2 state high spin intermediate that is able to advance to S_3 at temperatures as low as 180 K. The difference between this high spin state and that which is unable to advance at 180 K (the low spin S_2 state) is likely to be linked to its protonation state. The data are consistent with the prediction from several theoretical studies that the high spin form of S_2 is an obligate intermediate for advancement to S_3, however the experimental data alone do not rule out the possibility that the low spin form is unable to advance to S_3 at room temperature. Secondly, it provides evidence for a second form of S_3 which appears to be in equilibrium with the better studied form (the one which exhibits an EPR signal) and we argue that this indicates that it is not a precursor of this well-studied form of S_3 state. Thirdly, experimental evidence is provided that two forms of S_1 exist, those that are the precursors of the high and low spin forms of S_2. These new observations should be integrated into future theoretical models to improve understanding of these important steps in the cycle.

Transparency Document

The Transparency document associated with this article can be found, in the online version.

Acknowledgements

AB was supported in part by the French Infrastructure for Integrated Structural Biology (FRISBI) ANR-10-INSB-05-01 and the CEA/DSV "Bioénergie" program LOC1041OXYDO. AWR is a recipient of a Wolfson Merit Award from the Royal Society and is supported by a Biotechnology and Biological Sciences Research Council (BBSRC) grant BB/K002627/1. MS was supported by JST-PRESTO program (4018 for M.S.) and Grant-in-Aid for scientific research from the Ministry of Education, Science, Sports, Culture and Technology (21612007 for M.S.).

Appendix A. Supplementary data

Supplementary data to this article can be found online at http://dx.doi.org/10.1016/j.bbabio.2015.03.006.

References

[1] Y. Umena, K. Kawakami, J.-R. Shen, N. Kamiya, Crystal structure of oxygen–evolving photosystem II at a resolution of 1.9 Å, Nature 473 (2011) 55–60.
[2] F.H.M. Koua, Y. Umena, K. Kawakami, J.-R. Shen, Structure of Sr-substituted photosystem II at 2.1 angstrom resolution and its implications in the mechanism of water oxidation, Proc. Natl. Acad. Sci. U. S. A. 110 (2013) 3389–3894.

[3] A. Guskov, J. Kern, A. Gabdulkhakov, M. Broser, A. Zouni, W. Saenger, Cyanobacterial photosystem II at 2.9-angstrom resolution and the role of quinones, lipids, channels and chloride, Nat. Struct. Mol. Biol. 16 (2009) 334–342.

[4] B.A. Diner, F. Rappaport, Structure, dynamics, and energetic of the primary photochemistry of photosystem II of oxygenic photosynthesis, Annu. Rev. Plant Biol. 53 (2002) 551–580.

[5] G. Renger, Light-induced oxidative water splitting in photosynthesis: energetics, kinetics, and mechanism, J. Photochem. Photobiol. B 104 (2011) 35–43.

[6] H. Dau, I. Zaharieva, M. Haumann, Recent developments in research on water oxidation by photosystem II, Curr. Opin. Chem. Biol. 16 (2012) 3–10.

[7] B. Kok, B. Forbush, M. McGloin, Cooperation of charges in photosynthetic O_2 evolution—I. A linear four step mechanism, Photochem. Photobiol. 11 (1970) 457–475.

[8] P. Joliot, B. Kok, Oxygen evolution in photosynthesis, in: Govindjee (Ed.), Bioenergetics of Photosynthesis, Academic Press, New York 1975, pp. 387–412.

[9] N. Cox, J. Messinger, Reflections on substrate water and dioxygen formation, Biochim. Biophys. Acta 1827 (2013) 1020–1030.

[10] J. Yano, V. Yachandra, Mn_4Ca cluster in photosynthesis: where and how water is oxidized to dioxygen, Chem. Rev. 114 (2014) 4175–4205.

[11] M.R.A. Blomberg, T. Borowski, F. Himo, R.Z. Liao, P.E.M. Siegbahn, Quantum chemical studies of mechanisms for metalloenzymes, Chem. Rev. 114 (2014) 3601–3658.

[12] H. Isobe, M. Shoji, S. Yamanaka, H. Mino, Y. Umena, K. Kawakami, N. Kamiya, J.-R. Shen, K. Yamaguchi, Generalized approximate spin projection calculations of effective exchange integrals of the CaMn4O5 cluster in the S-1 and S-3 states of the oxygen evolving complex of photosystem II, Phys. Chem. Chem. Phys. 16 (2014) 11911–11923.

[13] A. Sedoud, N. Cox, M. Sugiura, W. Lubitz, A. Boussac, A.W. Rutherford, The semiquinone-iron complex of photosystem II: EPR signals assigned to the low field edge of the ground state doublet of $Q_A^{\bullet-}Fe^{2+}$ and $Q_B^{\bullet-}Fe^{2+}$, Biochemistry 50 (2011) 6012–6021.

[14] C. Fufezan, C.-X. Zhang, A. Krieger-Liszkay, A.W. Rutherford, Secondary quinone in photosystem II of *Thermosynechococcus elongatus*: semiquinone-iron EPR signals and temperature dependence of electron transfer, Biochemistry 44 (2005) 12780–12789.

[15] A. Boussac, A.W. Rutherford, Comparative study of the g = 4.1 EPR signals in the S_2-state of photosystem II, Biochim. Biophys. Acta 1457 (2000) 145–156.

[16] R. Pokhrel, G.W. Brudvig, Oxygen-evolving complex of photosystem II: correlating structure with spectroscopy, Phys. Chem. Chem. Phys. 16 (2014) 11812–11821.

[17] G.C. Dismukes, Y. Siderer, Intermediates of a polynuclear manganese center involved in photosynthetic oxidation of water, Proc. Natl. Acad. Sci. U. S. A. 78 (1981) 274–278.

[18] J.-L. Zimmermann, A.W. Rutherford, Electron paramagnetic resonance studies of the oxygen-evolving enzyme of photosystem II, Biochim. Biophys. Acta 767 (1984) 160–167.

[19] J.L. Casey, K. Sauer, Electron paramagnetic resonance detection of a cryogenically photogenerated intermediate in photosynthetic oxygen evolution, Biochim. Biophys. Acta 767 (1984) 21–28.

[20] J.C. de Paula, J.B. Innes, G.W. Brudvig, Electron-transfer in photosystem II at cryogenic temperatures, Biochemistry 24 (1985) 8114–8120.

[21] O. Horner, E. Rivière, G. Blondin, S. Un, A.W. Rutherford, J.-J. Girerd, A. Boussac, SQUID magnetization study of the infrared-induced spin transition in the S_2-state of photosystem II: spin value associated with the g = 4.1 EPR signal, J. Am. Chem. Soc. 120 (1998) 7924–7928.

[22] A. Boussac, S. Un, O. Horner, A.W. Rutherford, High spin states ($S \geq 5/2$) of the photosystem II manganese complex, Biochemistry 37 (1998) 4001–4007.

[23] P.E.M. Siegbahn, O–O bond formation in the S-4 state of the oxygen-evolving complex in photosystem II, Chem. Eur. J. 12 (2006) 9217–9227.

[24] P.E.M. Siegbahn, Structures and energetics for O2 formation in photosystem II, Acc. Chem. Res. 42 (2009) 1871–1880.

[25] P.E.M. Siegbahn, Recent theoretical studies of water oxidation in photosystem II, J. Photochem. Photobiol. B Biol. 104 (2011) 94–99.

[26] P.E.M. Siegbahn, Mechanisms for proton release during water oxidation in the S-2 to S-3 and S-3 to S-4 transitions in photosystem II, Phys. Chem. Chem. Phys. 14 (2012) 4849–4856.

[27] P.E.M. Siegbahn, Water oxidation mechanism in photosystem II, including oxidations, proton release pathways, O–O bond formation and O_2 release, Biochim. Biophys. Acta 1827 (2013) 1003–1019.

[28] K. Yamaguchi, H. Isobe, S. Yamanaka, T. Saito, K. Kanda, M. Shoji, Y. Umena, K. Kawakami, J.-R. Shen, N. Kamiya, M. Okumura, Full geometry optimizations of the mixed-valence CaMn4O4X(H2O)(4) (X = OH or O) cluster in OEC of PS II: degree of symmetry breaking of the labile Mn–X–Mn bond revealed by several hybrid DFT calculations, Int. J. Quantum Chem. 113 (2013) 525–541.

[29] N. Cox, D.A. Pantazis, F. Neese, W. Lubitz, Biological water oxidation, Acc. Chem. Res. 46 (2013) 1588–1596.

[30] D.A. Pantazis, W. Ames, N. Cox, W. Lubitz, F. Neese, Two interconvertible structures that explain the spectroscopic properties of the oxygen-evolving complex of photosystem II in the S_2 State, Angew. Chem. Int. Ed. 51 (2012) 9935–9940.

[31] W. Ames, D.A. Pantazis, V. Krewald, N. Cox, J. Messinger, W. Lubitz, F. Neese, Theoretical evaluation of structural models of the S_2 state in the oxygen evolving complex of photosystem ii: protonation states and magnetic interactions, J. Am. Chem. Soc. 133 (2011) 19743–19757.

[32] D. Bovi, D. Narzi, L. Guidoni, The S_2 state of the oxygen-evolving complex of photosystem II explored by QM/MM dynamics: spin surfaces and metastable states suggest a reaction path towards the S_3 State, Angew. Chem. Int. Ed. 52 (2013) 11744–11749.

[33] R. Pal, C.F.A. Negre, L. Vogt, R. Pokhrel, M.Z. Ertem, G.W. Brudvig, V.S. Batista, S-0-state model of the oxygen-evolving complex of photosystem II, Biochemistry 52 (2013) 7703–7706.

[34] A. Robertazzi, A. Galstyan, E.W. Knapp, Reprint of PSII manganese cluster: protonation of W2, O5, O4 and His337 in the S_1 state explored by combined quantum chemical and electrostatic energy computations, Biochim. Biophys. Acta 1837 (2014) 1389–1394.

[35] H. Isobe, M. Shoji, S. Yamanaka, Y. Umena, K. Kawakami, N. Kamiya, J.-R. Shen, K. Yamaguchi, Theoretical illumination of water-inserted structures of the $CaMn_4O_5$ cluster in the S_2 and S_3 states of oxygen-evolving complex of photosystem II: full geometry optimizations by B3LYP hybrid density functional, Dalton Trans. 41 (2012) 13727–13740.

[36] V. Krewald, M. Retegan, N. Cox, J. Messinger, W. Lubitz, S. DeBeer, F. Neese, D.A. Pantazis, Metal oxidation states in biological water splitting, Chem. Sci. 6 (2015) 1676–1695.

[37] R.D. Britt, K.A. Campbell, J.M. Peloquin, J.L. Gilchrist, C.P. Aznar, M.M. Dicus, J. Robblee, J. Messinger, Biochim. Biophys. Acta 1655 (2004) 158–171.

[38] L.V. Kulik, B. Epel, W. Lubitz, J. Messinger, Electronic structure of the Mn4OxCa cluster in the S_0 and S_2 states of the oxygen-evolving complex of photosystem II based on pulse Mn-55-ENDOR and EPR spectroscopy, J. Am. Chem. Soc. 139 (2007) 13421–13435.

[39] H. Dau, M. Haumann, Time-resolved X-ray spectroscopy leads to an extension of the classical S-state cycle model of photosynthetic oxygen evolution, Photosynth. Res. 92 (2007) 327–343.

[40] C. Glockner, J. Kern, M. Broser, A. Zouni, V. Yachandra, J. Yano, Structural changes of the oxygen-evolving complex in photosystem II during the catalytic cycle, J. Biol. Chem. 288 (2013) 22607–22620.

[41] R.J. Debus, FTIR Studies of Metal Ligands, Networks of Hydrogen Bonds, and Water Molecules near the Active Site Mn4CaO5 Cluster in Photosystem II, Biochim. Biophys. Acta 1847 (2015) 19–34.

[42] T. Noguchi, Fourier transform infrared difference and time-resolved infrared detection of the electron and proton transfer dynamics in photosynthetic water oxidation, Biochim. Biophys. Acta 1847 (2015) 35–45.

[43] H. Bao, P.L. Dilbeck, R. Burnap, Proton transport facilitating water-oxidation: the role of second sphere ligands surrounding the catalytic metal cluster, Photosynth. Res. 116 (2013) 215–229.

[44] A. Boussac, M. Sugiura, A.W. Rutherford, P. Dorlet, Complete EPR spectrum of the S_3-state of the oxygen-evolving photosystem II, J. Am. Chem. Soc. 131 (2009) 5050–5051.

[45] Y. Sanakis, J. Sarrou, G. Zahariou, V. Petrouleas, Recent EPR studies of the OEC of photosystem II. (A) Trapping tyrosyl Z center dot in action. (B) The critical S_3 integer-spin state of the Mn cluster in photosynthesis in energy from the sun, in: J.F. Allen, E. Gantt, J. Golbeck, B. Osmond (Eds.), 14th International Congress on Photosynthesis, Springer, Dordrecht, Netherlands 2008, p. 479.

[46] N. Cox, M. Retegan, F. Neese, D.A. Pantazis, A. Boussac, W. Lubitz, Electronic structure of the oxygen evolving complex in photosystem II prior to O–O bond formation, Science 345 (2014) 804–808.

[47] H. Nilsson, T. Krupnik, J. Kargul, J. Messinger, Substrate water exchange in photosystem II core complexes of the extremophilic red alga *Cyanidioschyzon merolae*, Biochim. Biophys. Acta 1837 (2014) 1257–1262.

[48] H. Nilsson, F. Rappaport, A. Boussac, J. Messinger, Substrate-water exchange in photosystem II is arrested prior to dioxygen formation, Nat. Commun. 5 (2014) 4305–4311.

[49] M. Retegan, N. Cox, W. Lubitz, F. Neese, D.A. Pantazis, The first tyrosyl radical intermediate formed in the S_2-S_3 transition of photosystem II, Phys. Chem. Chem. Phys. 16 (2014) 11901–11910.

[50] D. Narzi, D. Bovi, L. Guidoni, Pathway for Mn-cluster oxidation by tyrosine-Z in the S_2 state of photosystem II, Proc. Natl. Acad. Sci. U. S. A. 111 (2014) 8723–8728.

[51] A. Boussac, J.-J. Girerd, A.W. Rutherford, Conversion of the spin-state of the manganese complex in photosystem II induced by near-infrared light, Biochemistry 35 (1996) 6984–6989.

[52] A. Boussac, H. Kuhl, S. Un, M. Rögner, A.W. Rutherford, Effect of near-infrared light on the S_2-state of the manganese complex of photosystem II from *Synechococcus elongatus*, Biochemistry 37 (1998) 8995–9000.

[53] V. Petrouleas, D. Koulougliotis, N. Ioannidis, Trapping of metalloradical intermediates of the S-states at liquid helium temperatures. Overview of the phenomenology and mechanistic implications, Biochemistry 44 (2005) 6723–6728.

[54] K.G.V. Havelius, J. Sjoholm, F.M. Ho, F. Mamedov, S. Styring, Metalloradical EPR signals from the Y–Z center dot S-state intermediates in photosystem II, Appl. Magn. Reson. 37 (2010) 151–176.

[55] N. Ioannidis, J.H.A. Nugent, V. Petrouleas, Intermediates of the S_3 state of the oxygen-evolving complex of photosystem II, Biochemistry 41 (2002) 9589–9600.

[56] J.H. Su, H.K.V. Havelius, F.M. Ho, G. Han, F. Mamedov, S. Styring, Formation spectra of the EPR split signals from the S_0, S_1, and S_3 states in photosystem II induced by monochromatic light at 5 K, Biochemistry 46 (2007) 10703–10712.

[57] A. Boussac, M. Sugiura, T.-L. Lai, A.W. Rutherford, Low temperature photochemistry in photosystem II from *Thermosynechococcus elongatus* induced by visible and near-infrared light, Philos. Trans. R. Soc. 363 (2008) 1203–1210.

[58] A. Boussac, M. Sugiura, Y. Inoue, A.W. Rutherford, EPR study of the oxygen evolving complex in His-tagged photosystem II from the cyanobacterium *Synechococcus elongatus*, Biochemistry 39 (2000) 13788–13799.

[59] A. Boussac, N. Ishida, M. Sugiura, F. Rappaport, Probing the role of chloride in photosystem II from *Thermosynechococcus elongatus* by exchanging chloride for iodide, Biochim. Biophys. Acta 1817 (2012) 802–810.

[60] K. Saito, H. Ishikita, Influence of the Ca^{2+} ion on the Mn_4Ca conformation and the H-bond network arrangement in photosystem II, Biochim. Biophys. Acta 1837 (2014) 159–166.
[61] M. Sugiura, A. Boussac, T. Noguchi, F. Rappaport, Influence of Histidine-198 of the D1 subunit on the properties of the primary electron donor, P680, of photosystem II in *Thermosynechococcus elongatus*, Biochim. Biophys. Acta 1777 (2008) 331–342.
[62] M. Sugiura, Y. Inoue, Highly purified thermo-stable oxygen evolving photosystem II core complex from the thermophilic cyanobacterium *Synechococcus elongatus* having His-tagged CP43, Plant Cell Physiol. 40 (1999) (1219-123).
[63] N. Ishida, M. Sugiura, F. Rappaport, T.-L. Lai, A.W. Rutherford, A. Boussac, Biosynthetic exchange of bromide for chloride and strontium for calcium in the photosystem II oxygen-evolving enzyme, J. Biol. Chem. 283 (2008) 13330–13340.
[64] M. Sugiura, Y. Ozaki, N. Nakamura, N. Cox, F. Rappaport, A. Boussac, The D1-173 amino acid is a structural determinant of the critical interaction between D1-Tyr161 (TyrZ) and D1-His190 in photosystem II, Biochim. Biophys. Acta 1837 (2014) 1922–1931.
[65] A. Boussac, A.W. Rutherford, Nature of the inhibition of the oxygen-evolving enzyme of photosystem II induced by NaCl-washing and reversed by the addition of Ca^{2+} or Sr^{2+}, Biochemistry 27 (1988) 3476–3483.
[66] N. Cox, L. Rapatskiy, J.-H. Su, D.A. Pantazis, M. Sugiura, L. Kulik, P. Dorlet, A.W. Rutherford, F. Neese, A. Boussac, W. Lubitz, J. Messinger, The effect of Ca^{2+}/Sr^{2+} substitution on the electronic structure of the oxygen-evolving complex of photosystem II: a combined multi-frequency EPR, 55Mn-ENDOR and DFT study of the S_2 state, J. Am. Chem. Soc. 133 (2011) 3635–3648.
[67] A.R. Corrie, J.H.A. Nugent, M.C.W. Evans, Identification of EPR signals from the states $Q_A^-Q_B^-$ AND Q_B^- in photosystem II from *Phormidium laminosum*, Biochim. Biophys. Acta 1057 (1991) 384–390.
[68] A. Boussac, M. Sugiura, F. Rappaport, Probing the quinone binding site of photosystem II from *Thermosynechococcus elongatus* containing either PsbA1 or PsbA3 as the D1 protein through the binding characteristics of herbicides, Biochim. Biophys. Acta 1807 (2011) 119–129.
[69] S. Styring, A.W. Rutherford, In the oxygen-evolving complex of photosystem II the S_0 state is oxidized to the S_1 state by D^+ (signal II slow), Biochemistry 26 (1987) 2401–2405.
[70] D. Koulougliotis, J.-R. Shen, N. Ioannidis, V. Petrouleas, Near-IR irradiation of the S_2 state of the water oxidizing complex of photosystem II at liquid helium temperatures produces the metalloradical intermediate attributed to $S_1Y_Z^{\bullet}$ center, Biochemistry 42 (2003) 3045–3053.
[71] A. Boussac, M. Sugiura, D. Kirilovsky, A.W. Rutherford, Near-infrared-induced transitions in the manganese cluster of photosystem II: action spectra for the S_2 and S_3 redox states, Plant Cell Physiol. 46 (2005) 837–842.
[72] S. Styring, A.W. Rutherford, Deactivation kinetics and temperature-dependence of the S-state transitions in the oxygen-evolving system of photosystem-II measured by electron paramagnetic resonance spectroscopy, Biochim. Biophys. Acta 933 (1988) 378–387.
[73] Y. Sanakis, N. Ioannidis, G. Sioros, V. Petrouleas, A novel $S = 7/2$ configuration of the Mn cluster of photosystem II, J. Am. Chem. Soc. 123 (2001) 10766–10767.
[74] A. Boussac, F. Rappaport, P. Carrier, J.-M. Verbavatz, R. Gobin, D. Kirilovsky, A.W. Rutherford, M. Sugiura, Biosynthetic Ca^{2+}/Sr^{2+} exchange in the photosystem II oxygen evolving enzyme of *Thermosynechococcus elongatus*, J. Biol. Chem. 279 (2004) 22809–22819.
[75] A. Boussac, F. Rappaport, K. Brettel, M. Sugiura, Charge recombination in $S_nTyr_Z^{\bullet}Q_A^{-\bullet}$ radical pairs in D1 protein variants of photosystem II: long range electron transfer in the Marcus inverted region, Phys. Chem. B 117 (2013) 3308–3314.
[76] K. Kawakami, Y. Umena, N. Kamiya, J.-R. Shen, Location of chloride and its possible functions in oxygen-evolving photosystem II revealed by X-ray crystallography, Proc. Natl. Acad. Sci. U. S. A. 106 (2009) 8567–8572.
[77] C. Meinke, V.A. Sole, P. Pospisil, H. Dau, Does the structure of the water-oxidizing photosystem II–manganese complex at room temperature differ from its low-temperature structure? A comparative X-ray absorption study, Biochemistry 39 (2000) 7033–7040.
[78] F. Rappaport, J. Lavergne, Proton release during successive oxidation steps of the photosynthetic water oxidation process: stoichiometries and pH dependence, Biochemistry 30 (1991) 10004–10012.
[79] H. Suzuki, M. Sugiura, T. Noguchi, Monitoring proton release during photosynthetic water oxidation in photosystem II by means of isotope-edited infrared spectroscopy, J. Am. Chem. Soc. 131 (2009) 7849–7857.
[80] A. Klauss, M. Haumann, H. Dau, Alternating electron and proton transfer steps in photosynthetic water oxidation, Proc. Natl. Acad. Sci. U. S. A. 109 (2012) 16035–16040.
[81] W. Junge, M. Haumann, R. Ahlbrink, A. Mulkidjanian, J. Clausen, Electrostatics and proton transfer in photosynthetic water oxidation, Philos. Trans. R. Soc. B 357 (2002) 1407–1417.
[82] A. Klauss, M. Haumann, H. Dau, Seven steps of alternating electron and proton transfer in photosystem II water oxidation traced by time-resolved photothermal beam deflection at improved sensitivity, J. Phys. Chem. B 119 (2015) 2677–2689.
[83] P. Faller, C. Goussias, A.W. Rutherford, S. Un, Resolving intermediates in biological proton-coupled electron transfer: a tyrosyl radical prior to proton movement, Proc. Natl. Acad. Sci. U. S. A. 100 (2003) 8732–8735.
[84] K. Saito, J.-R. Shen, T. Ishida, H. Ishikita, Short hydrogen bond between redox-active tyrosine Yz and D1-His190 in the photosystem II crystal structure, Biochemistry 50 (2011) 9836–9844.
[85] K. Saito, A.W. Rutherford, H. Ishikita, Mechanism of tyrosine D oxidation in photosystem II, Proc. Natl. Acad. Sci. U. S. A. 110 (2013) 7690–7695.
[86] A. Boussac, Quantification of the number of spins in the S_2- and S_3-states of Ca^{2+}-depleted photosystem II by pulsed-EPR spectroscopy, Biochim. Biophys. Acta 1277 (1996) 253–266.
[87] J. Sjoholm, H.K.V. Havelius, F. Mamedov, S. Styring, Effects of pH on the S_3 state of the oxygen evolving complex in photosystem II probed by EPR split signal induction, Biochemistry 49 (2010) 9800–9808.
[88] M. Chrysina, G. Zahariou, N. Ioannidis, V. Petrouleas, Conversion of the $g = 4.1$ EPR signal to the multiline conformation during the S_2 to S_3 transition of the oxygen evolving complex of photosystem II, Biochim. Biophys. Acta 1797 (2010) 487–493.